INTERNATIONAL JOURNAL OF MARITIME TECHNOLOGY
IJMT Vol.16/ Summer 2021 (93-105)
Available online at: www. ijmt.ir

Determination of the Power Resonant Frequency of an OWC Converter Based on the RLC Circuit Analytical Approach

Abuzar Abazari[1*], Mohammad Reza Zarei[2], Saleheh Poursheikhali[3]

[1] *Faculty member of Chabahar Maritime University, abuzarabazari@cmu.ac.ir.*
[2] *Faculty member of Chabahar Maritime University, mrzarei@cmu.ac.ir.*
[3] *Faculty member of Chabahar Maritime University, s.poursheikhali@cmu.ac.ir.*

ARTICLE INFO

Article History:
Received: 22 May. 2022
Accepted: 17 Jul. 2022

Keywords:
wave energy converter
oscillating water column
power resonant frequency
free decay test
phase difference
RLC circuit

ABSTRACT

The oscillating water column is one of the most applicable and commercialized wave energy converters. There are some analytical-based simplified approaches like the rigid piston model for analyzing such converters in which the dynamic motion's damping, inertia, and stiffness are respectively modeled with a resistor, inductor, and capacitor (an RLC circuit). The power resonant frequency of wave energy converters is computed by solving the motion equation via its equivalent RLC circuit model. The free decay test is the other simple method for determining the resonant frequency and has been investigated experimentally. However, a comprehensive study is required. In this investigation, first, the effect of parameters like pressure, flow rate, and their phase difference on power resonant frequency, capture factor, etc., are conceptually investigated. Then, the relation between resonant frequency and free decay test frequency is studied for different chamber sizes. The results indicate that the free decay test frequency is generally close to the power resonant frequency.

1. Introduction

Wave energy is one of the renewable sources which has been increasingly the focus of researchers for producing electricity in recent years due to the global warming problems. Many types of wave energy converters have been proposed and analyzed in the basic design, the small-scale model, and the full-scale testing. The oscillating water column (OWC) converter is one of the successful designs investors have welcomed. Furthermore, this device has been commercialized as it requires few mechanical parts, resulting in low manufacturing costs and maintenance issues.

The OWC includes a hallowed chamber with just two open spaces, one at the top and one at the bottom. A turbine is located at the top of the chamber in an open orifice and plays the role of induced damping or generating power. Meanwhile, the open space at the bottom of the chamber encounters incident waves. Therefore, the pressured air above the water surface in the chamber can rotate the turbine, which is the exhalation step of the chamber. However, the air enters the chamber opposite the previous step during inhalation. However, the turbine is designed to create unidirectional rotational motion in both steps. This mechanical rotational motion is converted to electricity by a generator.

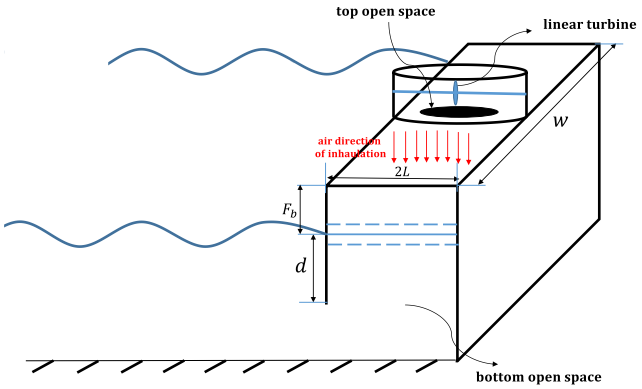

Figure 1. The oscillating water column with a rectangular chamber

One of the theory-based approaches related to OWC is a simplified analytical rigid piston model. In this method, the free surface level is considered a weightless piston moving vertically. The wavelength should be much enough to be able to consider a horizontal water level for deriving the equation of motion. Evans[1] calculated the efficiency of two OWC wave energy converters, including a design with vertical parallel plates and the other one with a narrow tube under wave excitation. Brendmo, et al. [2] modeled a pneumatic power take-off type of an OWC,

and a Mass-Spring-Damper (MSD) equivalent model was presented. They modeled the viscous energy loss by defining a mechanical loss resistance.

Furthermore, a mathematical model was presented by Lopes, et al. [3] for a case study with a lower OWC diameter and wave amplitude compared to the wavelength and the draft, respectively. Falcao [4] conducted an analytical-based hydrodynamic analysis for a floating OWC consisting of an axisymmetric tube fixed in a floater. The proposed simplified model investigated the effect of utilizing a non-uniform inner cross-section. Ketabdari et al. [5] considered a thin, rigid plate as a model for water surface level. They used ship hydrodynamic theories to investigate the radiation condition of a plate motion and the diffraction condition of a fixed OWC. After calculating the exciting force and hydrodynamic coefficients, the air pressure has been computed.

If the governing equation is linear, an analytical solution can be presented. It is worth noting that the approximated linear terms of the radiation forces, including the added mass and radiation damping forces, are expressed by hydrodynamic coefficients. There are also analytical methods to derive the coefficients for simplified shapes which are classified into two categories: first, the eigenfunction expansion approach [6, 7], and second, matched eigenfunction expansions approach [8, 9]. It should be noted that, as in the OWC case, solving linear governing equations in the frequency domain is generally conducted by applying an equivalent RLC electrical circuit. In the references of [10-13], an equivalent RLC model was obtained to analyze the linear equations obtained from wave energy converters. In the current study, we use an equivalent RLC model to solve equations and determine the system's unknown parameters like water level displacement and consequently the pressure, flow rate, capture factor. More details about the concept of the RLC circuit are described in section 3 of the present paper.

By solving the governing equations analytically, the generated power can be computed. One of the crucial points is the value of the power resonant frequency which can be obtained from the curve that shows the variation of the power versus frequency. This is an essential point because the dominant wave frequency of each location is specified, and it is significant to match the resonant frequency of the power extraction with the dominant wave frequency. On the other hand, calculating the extracted power is a long process to find out the value of the resonant frequency. In this regard, the simple free decay test approach has been suggested by several researchers just to determine the turbine-damping and the frequency of the water level displacement which are pointed in flowing.

A free decay test through Open-Foam numerical CFD simulation of a fixed OWC has been conducted by Simonetti, et al. [14] to find the frequency of the water surface motions. Vyzikas, et al. [15] simulated the free decay test of a fixed OWC converter with and without PTO to find the frequency of the water level oscillations with a RANS-type two-phase CFD model. Elhanafi, et al. [16] also derived the time–series and the spectral density of free decay tests for six types of OWC models to find the frequency of free vibrations. Furthermore, a mathematical vibration model was proposed by Çelik and Altunkaynak [17] for estimating the water level oscillations. Resistive forces against the water surface motion were supposed to be induced by the damping coefficient in the equations, which, in turn, have been determined experimentally. The results showed that the experimental and the mathematical model data are approximately similar. Moreover, they conducted experimental and 3D numerical free decay tests for an OWC with different opening heights and PTO characteristics [18]. The logarithmic decrement approach has computed the linear damping of OWC.

Furthermore, natural and resonant frequencies of the water level displacement and added mass have been calculated. They also evaluated the hydrodynamic characteristics such as hydrodynamic coefficients and the natural and resonant frequency of a fixed OWC at different underwater openings and orifice sizes via the concept of the logarithmic decrement approach experimentally[19]. Portillo, et al. [20] also carried out the free decay test to obtaine the natural heave, surge and pitch period for two WECs like the coaxial-duct and the spar-buoy types.

It has been observed from the previous studies that there is not a comprehensive comparison between the power resonant frequency, the free vibrational frequency of the water column, and other defined frequencies at different conditions, even in experimental-based research. For that, this study investigates the relation between power resonant frequency and calculated frequencies from the free decay test and the forced vibration at different sizes of the chamber based on the simplified piston model analytical approach.

This paper is organized as follows: Section 2 presents a mathematical model of the rigid piston model. In section 3, an equivalent RLC circuit model of the system is explained. Section 4 discusses the power and capture factor. Section 5 assign to the free decay test. Discussion and results are presented in section 6. Finally, section 7 concludes the paper.

2. Mathematical model

The schematic of the considered OWC wave energy converter is depicted in

Figure 1. The characteristic values of the chamber and well's turbine, presented in Table 1 are the same as the study of Simonetti, et al. [14]. However, here the chamber is assumed to be rectangular.

One of the strategies for simulating the OWC is the simplified rigid piston model, which helps a designer develop such a technology in the initial design steps. If the chamber is fixed, the motion equation is SDOF. The

linear airy wave theory based on the incompressible and irrotational flow is used to model the wave through the mathematical harmonic expressions.

Table 1. Characteristic values of the different parts of the oscillating water column converter

Parameter	Description	value	unit
N	Turbine rotational speed	50	Rad/s
D	Turbine diameter	1.75	m
K	Turbine flow/Pressure constant	0.28	…
ρ_w	Water density	1025	Kg/m^3
ρ_a	Air density	1.25	Kg/m^3
h	Water depth	50	m
ω	Wave frequency	0-1.8	Rad/s
d	OWC front wall draught	6-14	m
F_b	OWC freeboard	7.5	m
$2L$	Chamber length	6-14	m
H	Wave height	1	m

Suppose the chamber dimensions in the wave direction are smaller than the wavelength. In that case, the vertical reciprocating motion of the water-free surface inside the chamber, like a rigid piston movement, is a reliable assumption [7-10]. This reciprocating motion is the response of the SDOF-MSD mathematical model due to the wave excitation force. Therefore, the second law of newton applied on water column mass is as

$$m\ddot{x} = f_{froude-krylof} + f_{rad} + f_{hydst} + f_{air} \quad (1)$$

where $f_{froude-krylov}$, f_{rad}, f_{hydst} and f_{air} are the Froude-Krylov force due to the incident wave, radiation wave force, hydrostatic force, and the applied air pressure force on the rigid model of the water column, respectively. The considered mass of the oscillating water column is changing due to the fluctuation of the free surface; however, the variable part is relatively small compared to the constant part. Therefore, the time-varying part can be removed to simplify the equation [17]. The mentioned forces are calculated as follows. Regarding the linear wave theory, the wave surface elevation is expressed as

$$\eta_{wave} = \frac{H}{2}\cos(kx - \omega t) \quad (2)$$

The dynamic pressure is derived based on the solution of the Laplacian equation of the non-viscous protentional flow due to the undisturbed incident wave. It is expressed as

$$p_{wave} = \rho_w . g . \eta_{wave} . \frac{\cos(k(h+z))}{\cos(kh)} \quad (3)$$

where ρ_w is the water density, g is the gravity acceleration, k is the wavenumber, h is the water depth. The wavenumber can be calculated via dispersion relation as

$$\omega^2 = k . g . \tanh(kh) \quad (4)$$

Therefore, due to the incident wave, the Froude-Krylov force is the hydrodynamic pressure force applied to the water column [21]

$$f_{fr} = \eta_{wave} . S . \rho_w . g . \frac{\cos(k(h-d))}{\cos(kh)} \quad (5)$$

where S is the surface area of the water column or the cross-section area of the chamber.
The radiation wave through the oscillations of the water-free surface level inside of the chamber induces the added mass and radiation damping force.

$$f_{rad} = -m_a\ddot{z} - B_r\dot{z} \quad (6)$$

In the present study, the added mass and radiation damping are calculated based on the linearized frequency domain analysis of the potential flow analytical theory [1]. Evans calculated these coefficients for an oscillating water column between two thin vertical plates through the assumption of a weightless piston as

$$\frac{m_a}{M} = 1 + \frac{1}{\pi}\left(\frac{L}{d}\right)\left[\log\left(\frac{2\pi d}{L}\right) + 1 - 2e^{-2kd}\mathrm{Ei}(2kd)\right] \quad (7)$$

$$\frac{B_r}{M\omega} = 2\left(\frac{L}{d}\right)e^{-2kd} \quad (8)$$

where $M = 2Lwd\rho_w$ is the mass of the water column in the rectangular cuboid chamber. Noted that m_a and B_r define the added mass and radiation damping, respectively. Moreover, Ei is the exponential integral.

$$\mathrm{Ei}(2kd) = -\int_{-2kL}^{\infty}\frac{e^{-u}}{u}du \quad (9)$$

The variation of the hydrodynamic coefficients versus frequency at different sizes of the chamber is depicted in Figure 2. It is indicated that the smallest added mass of the oscillating water column is for the case with smallest value of front wall draught (d) and length ($2L$). As predicted, the results show that the chamber length is more effective than the draught on the added mass (Figure 2-a). The reason is that the cross-section area of the water column increase and can accelerate more fluid particles, consequently inducing more equivalent added mass. It is clear that the rise in the draught cannot considerably affect the added mass due to their same horizontal cross-section area. The added mass is approximately constant at high frequencies.

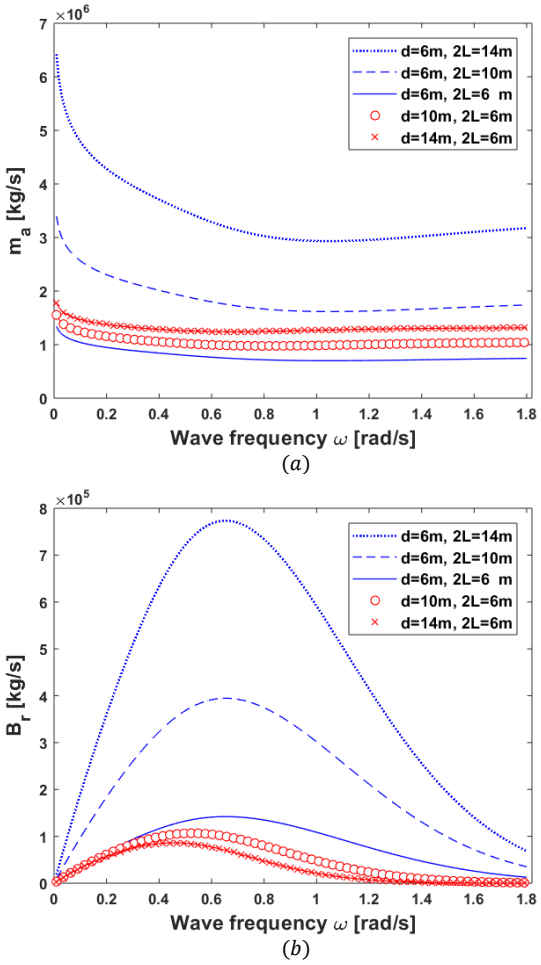

Figure 2. The variation of a) added mass and b) radiation damping versus frequency at the different sizes of the chamber

On the other hand, the radiation damping increase with the increase of the chamber length and reduces with the increase of OWC front wall draught as shown in Figure 2-b. Moreover, there is a peak frequency for the radiation damping, which decreases with the rise in the chamber draught. It is noted that these coefficients are not dependent on the value of the free surface level.
The applied hydrostatic force is due to the restoring force as in equation (10) which induces the hydrostatic stiffness to the OWC dynamic equation of motion.

$$f_{hst} = -\rho_w g A z = -K_{hst} z \tag{10}$$

f_{air} is the air pressure force applied to the water column. It is related to the air force due to the compressed air above the water free surface applied on the rigid model of the water column. As f_{air} is directly dependent on te induced hydrodynamic properties of the turbine installed on the top open space, it can be defined as the turbine force F_{Turb}. This force can be calculated as below:

$$f_{Turb} = -S.p_a \tag{11}$$

p_a is the air pressure difference between of the chamber and atmosphere. The air can be modeled as an ideal gas that acts in the isentropic process. The adiabatic thermodynamic process is assumed for analyzing the air governing equation related to the fact that heat exchanging in a wave period cycle is small. Moreover, the filling and discharging process are slow enough for the thermodynamic state of the air chamber [22]. Therefore, the mass airflow rate is approximated to a linear form as:

$$\dot{m} = \rho_a q - V_0 \frac{1}{C^2}\frac{dp_a}{dt} \tag{12}$$

where C is the sound speed in the air, V_0 is the air volume above the water column in the undisturbed condition. The flow rate crossing of the turbine is defined as $q = -\frac{dV_0}{dt}$. In a linear turbine, the mass airflow rate ($\dot{m}$) and pressure have a linear relationship [23, 24]. Therefore, the relation between p_a and q is written as

$$\frac{KD}{N}p_a + \frac{V_0}{C^2}\frac{dp_a}{dt} = \rho_a q \tag{13}$$

where K is turbine flow/pressure constant and N is turbine rotational speed. The air volume flow rate crossing the turbine is approximated via the change rate of the chamber volume above the free surface as the product of the cross-section area by the surface elevation velocity as

$$q(t) = -\frac{dV_0}{dt} = -(-\dot{z}.S) = Qe^{i\omega t} = i\omega S Z e^{i\omega t} \Rightarrow \quad Q = Si\omega Z \tag{14}$$

It can be concluded that both equations (1) and (13) are linear and can be written in the frequency domain as below. For solving the governing equation in the frequency domain, the free surface evaluation and pressure are considered complex harmonic variables as

$$z(t) = Ze^{i\omega t} \tag{15}$$

$$p_a(t) = Pe^{i\omega t} \tag{16}$$

Therefore, the equations (1) and (13) can be, respectively, written in the frequency domain as

$$-m\omega^2 Z - m_a\omega^2 Z + i\omega B_r Z + K_{hst} Z + S.P = F_{fr} \tag{17}$$

$$\frac{KD}{N}P + i\omega\frac{V_0}{C^2}P = \rho_a(Q) \xrightarrow{Q=S\omega iZ} P = \left(\frac{KD}{N} + i\omega\frac{V_0}{C^2}\right)^{-1}\rho_a Q = \Lambda Q \quad or \quad P = \frac{-\rho_a S\omega i}{\frac{KD}{N}+\frac{V_0}{C^2}\omega i} Z \tag{18}$$

where F_{fr} is the the Froude-Krylov force amplitude. By determining P versus Q based on equation (18), the

term related to air pressure force $(+S.P)$ at left hand side of equation (17) is decomposed into two different parts, which are conceptually named induced turbine virtual mass and damping. The first one is a coefficient multiplied by $i\omega Z$ which is interpreted as a turbine additional damping through turbine applied on the piston model. The second term is a coefficient multiplied by $-\omega^2$ which induces a virtual mass through turbine applied on the supposed piston model. These terms are presented in equations

$$S.P = S.\left(\frac{\rho_a S\omega i}{\frac{KD}{N}+\frac{V_0}{C^2}\omega i} Z\right) = +\rho_a S^2\omega.\left(\frac{\left(\frac{KD}{N}i+\frac{V_0}{C^2}\omega\right)}{\left(\frac{KD}{N}\right)^2+\left(\frac{\omega V_0}{C^2}\right)^2} Z\right) = \omega i B_{Turb} Z - (m_{Turb})\omega^2 Z \quad (19)$$

$$B_{Turb} = \frac{S^2\frac{KD}{N}\rho_a}{\left(\frac{KD}{N}\right)^2+\left(\frac{\omega V_0}{C^2}\right)^2} \quad (20)$$

$$m_{Turb} = -\frac{\frac{S^2 V_0}{C^2}\rho_a}{\left(\frac{KD}{N}\right)^2+\left(\frac{\omega V_0}{C^2}\right)^2} \quad (21)$$

This means the amplitude of the pressure force, $S.P$, at the left-hand side of the equation (17) can be expressed as $-m_{Turb}\omega^2+B_{Turb}i\omega$. Therefore, the motion equation can be rearranged as an equivalent SDOF-MSD with frequency-dependent coefficients as

$$[-(m+m_a+m_{Turb})\omega^2+(B_r+B_{Turb})i\omega+K_{hst}]Z = F_{fr} \quad (22)$$

The positive sign of the B_{Turb} justify the conceptual point that the induced damping by the turbine should resist the movement of the free surface level. On the other hand, if the term of the air pressure force on the left-hand side of the motion equation has the positive sign as $-S.P$, this cannot justify the mentioned crucial point. This approach explains that the procedure is conceptually correct.

As depicted in Figure 3 the turbine induced virtual mass and damping increase with the rise of chamber length or air volume above the free surface level. On the other hand, the chamber draught does not affect the resulting turbine-induced hydrodynamic coefficients. Generally, both of the defined hydrodynamic coefficients reduce versus frequency. All the coefficients in equation (22) are known and can be solved. Therefore, the frequency response at a steady-state situation is calculated as

$$Z = \frac{F_{fr}}{-(m+m_a+m_{Turb})\omega^2+(B_r+B_{Turb})i\omega+K_{hst}} = |Z|.e^{-i\theta} \quad (23)$$

where the amplitude and phase difference relative to the excitation force can be defined as

$$|Z| = \frac{F_{fr}}{[(K_{hst}-(m+m_a+m_{Turb})\omega^2)^2+(B_r+B_{Turb})^2\omega^2]^{\frac{1}{2}}} \quad (24)$$

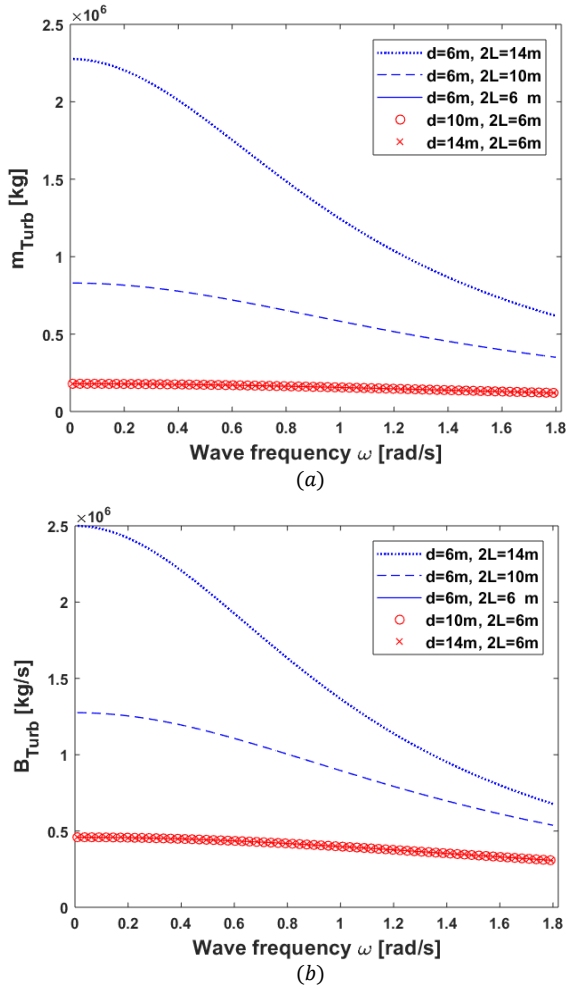

Figure 3. The variation of the induced a) virtual mass and b) damping of the turbine versus frequency at the different sizes of the chamber

$$\theta = \tan^{-1}\frac{(B_r+B_{Turb})\omega}{K_{hst}-(m+m_a+m_{Turb})\omega^2} \quad (25)$$

After calculating Z, the pressure and flow rate amplitude can also be determined via equations (14) and (18). As mentioned previously, the linear equation of the motion of an SDOF-MSD model can be solved by an equivalent electrical circuit.

3. Equivalent RLC circuit model

In this section, we aim to derive the circuit model of the obtained motion equation b by applying Ohm's law. In this way, the physical quantities are converted into electrical components, and an equivalent RLC circuit model is derived. For that, the wave excitation force and the free surface velocity are modeled by voltage drop and current, respectively. The complete conversion relation list is illustrated in Table 2.

Table 2. The electrical equivalent of the physical quantity

Physical quantity	Electrical quantity	Equivalence	Units
F	U	$F \leftrightarrow U$	$N \leftrightarrow V$
$B\dot{z}$	$U_R = RI$	$B \leftrightarrow R$	$Ns/m \leftrightarrow \Omega$
$M\ddot{z} = jwM\dot{z}$	$U_L = jwLI$	$M \leftrightarrow L$	$kg \leftrightarrow H$
$kz = (jw/k)^{-1}\dot{z}$	$U_C = \frac{I}{jwC}$	$1/k \leftrightarrow C$	$N/m \leftrightarrow F$

According to Table 2 the velocity of the free surface level is modeled with the current of the circuit; thus, the coefficients of $z, \dot{z}, \ddot{z}$ can be converted to capacitor, resistor, and inductor quantities, respectively.

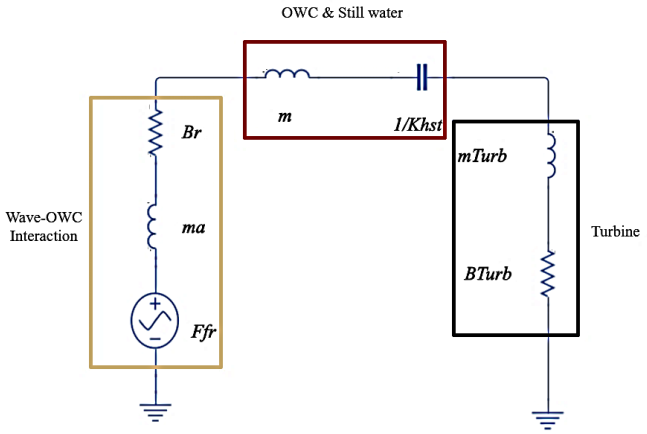

Figure 4. Equivalent RLC circuit model for the OWC

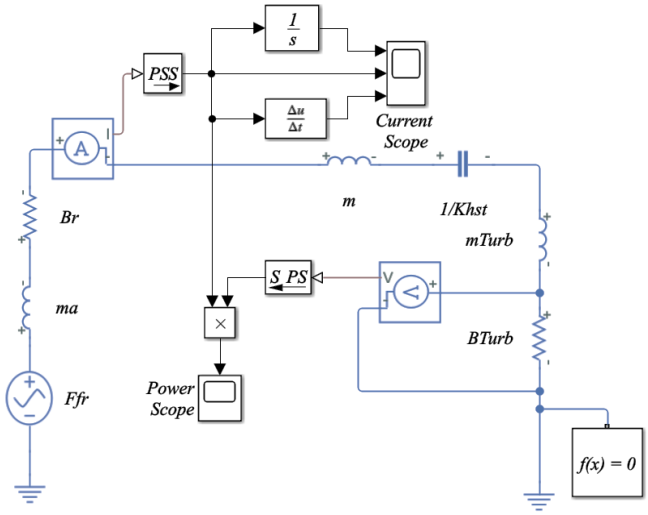

Figure 5. Equivalent electrical circuit model in Matlab Simulink

In addition, the damping coefficient, the equivalent mass, and the inverse of hydrostatic stiffness can be modeled with a resistor, an inductor, and a capacitor, respectively. As each term in the equation of motion is equivalent to a voltage drop, all terms of an equation can be considered to connect in series. In this way, a schematic view of the circuit model of the free surface level is displayed in Figure 4. It includes three principal parts. First, the wave-OWC interaction exhibits the interaction of wave on OWC comprising of the force due to the radiated wave and Froude Krylov. Second, the parts relate to the interaction of water column mass and its hydrostatic stiffness with still water. Third, the effect of the turbine as its induced virtual mass and damping on OWC. Moreover, the block diagram of the equivalent circuit model in Matlab-Simulink is presented in Figure 5. It should be noted that an equivalent RLC circuit model approach can be applied just for a vibrational system with linear motion equations.

4. Power and Capture factor

The hydrodynamic performance of an OWC wave energy converter is identified by captured power. Based on the linearity of the wave and PTO damping (wells turbine damping), the averaged output power is calculated as

$$\bar{P_o} = \frac{1}{T}\int_0^T q(t)\,p(t)dt \tag{26}$$

The capture factor is a well-known parameter in the investigation of the wave energy converter performance, which is defined as the power absorbed by OWC divided by the available input power of the wave as

$$C_f = \frac{\bar{P_o}}{w * P_w} \tag{27}$$

P_w is the averaged power per unit width, and w is the width of the imagined long crest wave matched with the width of the OWC device. By considering the linear airy wave theory, the averaged wave power per unit width is calculated via the following steps

$$P_w = E.C_g \tag{28}$$

$$E = \frac{\rho g H^2}{8} \tag{29}$$

$$C_g = \frac{\omega}{2k}\left[1 + \frac{2kh}{\mathrm{Sinh}\,(2kh)}\right] \tag{30}$$

$$P_w = \frac{\rho g H^2}{16}\frac{\omega}{k}\left[1 + \frac{2kh}{\mathrm{Sinh}(2kh)}\right] \tag{31}$$

Generally, the averaged output power of an OWC is the integral of flow rate product by pressure. Sometimes these parameters are unknown. For that, the other forms of the power formula are developed versus the other specified variables. These formulas are proved in the complex form as below. The first one is the relation of the output power to the turbine damping and maximum velocity as equation (32).

$$\begin{aligned}
&\overline{P_o} = \frac{1}{T}\int_0^T \text{Real}\left(Qe^{i\omega t}\right) * \text{Real}\left(Pe^{i\omega t}\right)dt = \\
&\frac{1}{T}\int_0^T \text{Real}\left(S\omega i|Z|.e^{-i\theta}e^{i\omega t}\right) * \\
&\text{Real}\left(\frac{\rho_a S}{\frac{KD}{N}+\frac{V_0}{C^2}\omega i}\omega i|Z|.e^{-i\theta}e^{i\omega t}\right)dt \\
&= \frac{1}{T}\int_0^T [S\omega|Z|.\text{Sin}(\omega t-\theta)] * \\
&\left[\frac{S\rho_a\frac{KD}{N}}{\left(\frac{KD}{N}\right)^2+\left(\frac{\omega V_0}{C^2}\right)^2}.\omega|Z|\,\text{Sin}(\omega t-\theta) - \right. \\
&\left.\frac{S\rho_a\frac{\omega^2 V_0}{C^2}}{\left(\frac{KD}{N}\right)^2+\left(\frac{\omega V_0}{C^2}\right)^2}.|Z|\,\text{Cos}(\omega t-\theta)\right]dt \\
&= \frac{1}{T}\int_0^T \omega|Z|.\text{Sin}(\omega t-\theta) * \\
&(B_{Turb}\omega|Z|\,\text{Sin}(\omega t-\theta) + \\
&m_{Turb}\omega^2|Z|\,\text{Cos}(\omega t-\theta))\,dt = \\
&\frac{1}{2}\,B_{Turb}\omega|Z|.\omega|Z| = \frac{1}{2}B_{Turb}\left|\omega|Z|\right|^2 = \\
&\frac{1}{2}B_{Turb}|\max(\dot{z}(t))|^2
\end{aligned} \tag{32}$$

As observed in the inertia term, $m_{Turb}\omega^2|Z|\,\text{Cos}(\omega t-\theta)$, is an orthogonal mode compared to the flow rate mode, $\omega|X|.\text{Sin}(\omega t-\theta)$. On the other hand, the phase difference is $\frac{\pi}{2}$ and the induced inertia term does not directly affect the output power of the power take-off system. However, the turbine-induced virtual mass can affect the maximum velocity, which, in turn, influences the output power. The averaged output power can be defined in equation (33) in terms of the turbine's characteristic values and hydrodynamic coefficients. This equation is obtained through the substitution of the B_{air} and $\max(\dot{x}(t))$ into equation (32).

$$\begin{aligned}
&\overline{P_o} = \frac{1}{2} * \frac{S^2\frac{KD}{N}\rho_a}{\left(\frac{KD}{N}\right)^2+\left(\frac{\omega V_0}{C^2}\right)^2} * \\
&\frac{\left[2.\omega.\eta_{wave}.S.\rho_w.g.\frac{\cos(k(h-L))}{\cos(kh)}\right]^2}{[(K_{hst}-(m+m_a+m_{air})\omega^2)^2+(B_r+B_{air})^2\omega^2]}
\end{aligned} \tag{33}$$

There is another formula for the power that can be expressed in terms of the amplitude of the pressure and the characteristic values of the turbine as in equation (34).

$$\begin{aligned}
&\overline{P_o} = \frac{1}{T}\int_0^T \text{Real}\left(Qe^{i\omega t}\right) * \text{Real}\left(Pe^{i\omega t}\right)dt = \\
&\frac{1}{T}\int_0^T \text{Real}\left\{\left(\frac{KD}{\rho_a N}+i\omega\frac{V_0}{\rho_a C^2}\right)P.e^{i\omega t}\right\} * \\
&\text{Real}\left(|P|.e^{\left(-\theta-\theta_1+\frac{3\pi}{2}+\omega t\right)i}\right)dt \\
&= \frac{1}{T}\int_0^T \text{Real}\left\{\left(\frac{KD}{\rho_a N}\right.\right. \\
&\left.\left.+\,i\omega\frac{V_0}{\rho_a C^2}\right).|P|.e^{\left(-\theta-\theta_1+\frac{3\pi}{2}+\omega t\right)i}\right\} \\
&* \text{Real}\left(|P|.e^{\left(-\theta-\theta_1+\frac{3\pi}{2}+\omega t\right)i}\right)dt \\
&= \frac{1}{T}\int_0^T |P|^2.\left[\frac{KD}{\rho_a N}\text{Cos}\left(\omega t-\theta-\theta_1+\frac{3\pi}{2}\right) - \right. \\
&\left.\omega\frac{V_0}{\rho_a C^2}\text{Sin}\left(\omega t-\theta+\frac{3\pi}{2}\right)\right] * \text{Cos}(\omega t-\theta - \\
&\theta_1+\frac{3\pi}{2}))\,dt == \frac{1}{2}\,\frac{KD}{\rho_a N}|P|^2
\end{aligned} \tag{34}$$

5. Free decay test

Suppose the excitation wave is not applied on the OWC. In that case, the motion of the free surface level can be observed through an initial displacement from the equilibrium position during the free oscillation. This is similar to the free vibration of an SDOF-MSD model. Since the damping force due to the radiated wave and wells turbine is applied during the free vibration of the surface level, the vibration amplitude decays versus time. It is noted that in real conditions, viscous damping has also existed, which is neglectable compared to the radiation and the turbine damping. Therefore, this test is called the free decay test, and the related dynamic motion and the response are expressed as

$$(m+m_a+m_{Turb})\ddot{z}(t) + (B_r + B_{Turb})\dot{z}(t) + K_{hst}.z(t) = 0 \tag{35}$$

$$\Rightarrow z(t) = Z_0 e^{-\zeta\omega_n t}Cos(\omega_d t+\phi_0) \tag{36}$$

The value of Z_0 and ϕ_0 are only dependent on the initial condition. If the dynamic characteristic values of the vibrational system are specified, the damped vibrational frequency of the free surface motion is defined as

$$\omega_d = \omega_n\sqrt{1-\zeta^2} \tag{37}$$

where the natural frequency and the damping ratio are determined as

$$\omega_n = \sqrt{K_{hst}/(m+m_a+m_{Turb})} \tag{38}$$

$$\zeta = \frac{B_r+B_{air}}{2\sqrt{K_{hst}.(m+m_a+m_{Turb})}} \tag{39}$$

However, as B_r, B_{air}, m_a and m_{air} are frequency-dependent, the theoretical vibrational frequency in the free decay test is calculated from equation (37) via an iteration method.

On the other hand, if only the free variation curve of the free surface, z, versus time is presented, as in Figure 6, the damping ratio and the natural frequency can be calculated from the logarithmic decrement of the vibration amplitudes and vibrational period, respectively, as expressed in equations (40) and (41). It should be emphasized that the damped natural frequency is determined from the measurement of the damped period, as shown in Figure 6. In practical conditions, the OWC frequency can be evaluated by imposing a load on the OWC chamber as the specified initial water level. The water level of the OWC

chamber is recorded to obtain the time history of water surface oscillations.

$$\Rightarrow Ln\frac{Z_n}{Z_{n+1}} = \frac{2\pi\zeta}{\sqrt{1-\zeta^2}} \quad (40)$$

$$\omega_d = \frac{2\pi}{\tau_d} = \omega_n\sqrt{1-\zeta^2} \Rightarrow \omega_n = \frac{2\pi}{\tau_d\sqrt{1-\zeta^2}} \quad (41)$$

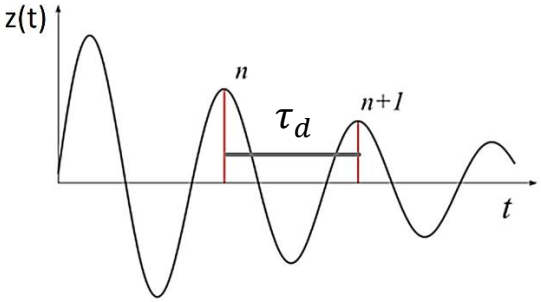

Figure 6. Free surface displacement versus time

This section aims to compare the natural frequency of the forced vibration with the damped frequency of the free decay test and the resonant frequency of the displacement, power, pressure, and flow rate.

The natural frequency of the forced vibration is defined as the root of the equivalent stiffness divided by the equivalent mass in each excitation frequency. The trend of this parameter versus the wave frequency is depicted in Figure 13 for different chamber sizes in the results section.

Noted that the free decay test can be conducted in the condition that the top of the rectangular chamber does not exist, which means the $+m_{Turb}$ and B_{Turb} are removed from the motion equation. The calculated damped frequency in this practical situation is indicated as "open top". In a specified theoretical condition, the equation of motion at the free decay test is modeled just by PTO damping (turbine damping) without the effect of the induced turbine virtual mass and even the radiation damping. This is the other case where the calculated damped frequency is called "Theory-only B_{Turb}" which is the based equation of some researchers for analyzing their problem.

6. Results and Discussion

By solving the frequency response equation (24), the variation of the free surface level versus frequency for various sizes of the rectangular chamber is presented in Figure 7. It is similar to the frequency response curves of an SDOF-MSD model. It indicates that the displacement amplitude of the water surface decreases with the increase of the chamber length. It is related to the resistance damping force induced by damping, which is high at high values of the chamber length. However, the larger front wall draught causes smaller values for motion amplitude of the free surface after resonance. As demonstrated in Figure 2 and Figure 3, the induced radiation, turbine virtual mass, and damping are not considerably affected by the draught increase. The considered mass of the water column and the excitation force are, respectively, increased and decreased by increasing the draught. This is the reason for reducing the displacement amplitude at the larger draught.

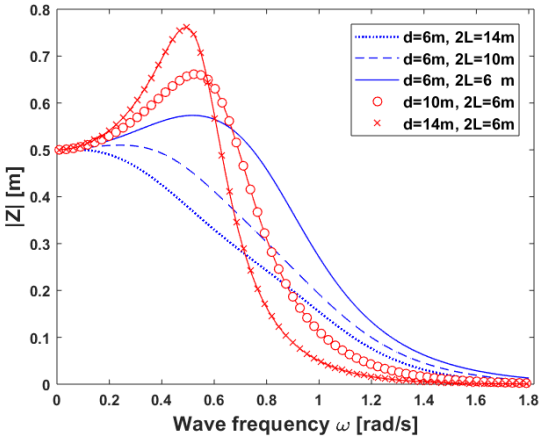

Figure 7. The variation of water level displacement at different sizes of the chamber

One of the objectives of this study is to find the relation between the resonant frequency of the pressure, flow rate, water displacement, and power. This matter is investigated in the following.

After calculating the free surface displacement, the variation of the pressure amplitude inside the chamber and the flow rate amplitude can be concluded based on the equations (14) and (18) as shown in Figure 8. It is observed that the resonance frequency of Q and P are approximately the same for a specified dimension of the chamber. The increase of the chamber length causes a wideband frequency response of the pressure and the flow rate around the peak. Since the averaged output power is the integral of the multiplication of $q(t)$ and $p(t)$, the frequency-dependent wideband power is expected to be derived at larger values of the chamber length. This point is confirmed in the curve of the averaged output power as in Figure 9-a. It should be noted that the increase of the chamber length or front wall draught decreases the resonance frequency of pressure, flow rate, and output power, and the effect of both these variables on changing the resonance point is approximately the same. It is concluded that for practical applications, in a sea state with long wave periods or low wave frequencies, the chamber should be large enough to be able to match the power resonance frequency with dominant large wave periods. This is set by an increase in the length or front wall draught.

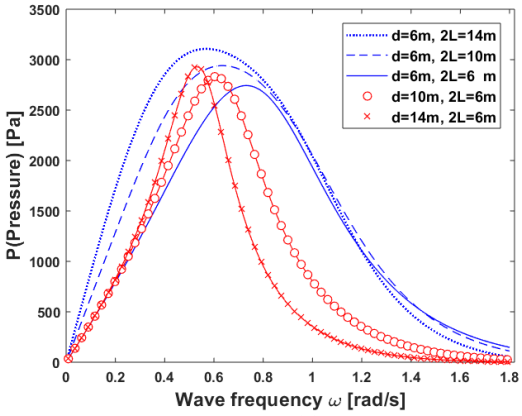

(a)

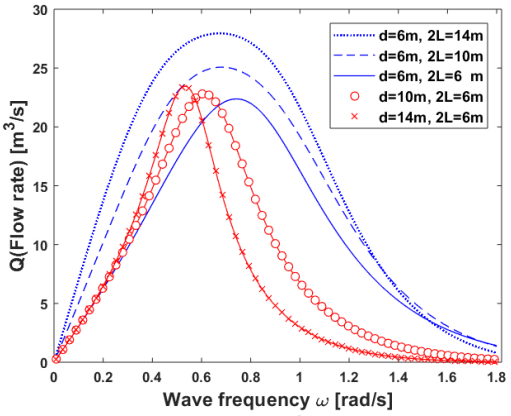

(b)

Figure 8. The variation of a) the pressure amplitude and b) the flow rate amplitude versus frequency at different chamber sizes

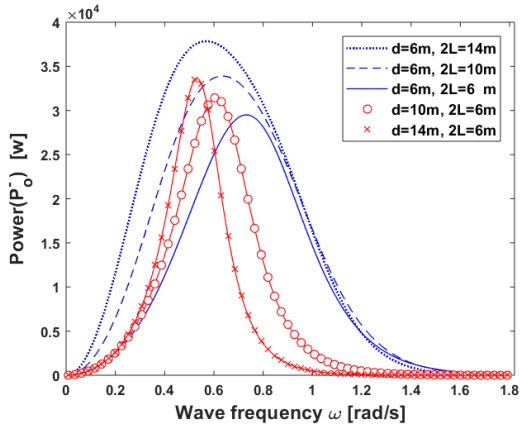

(a)

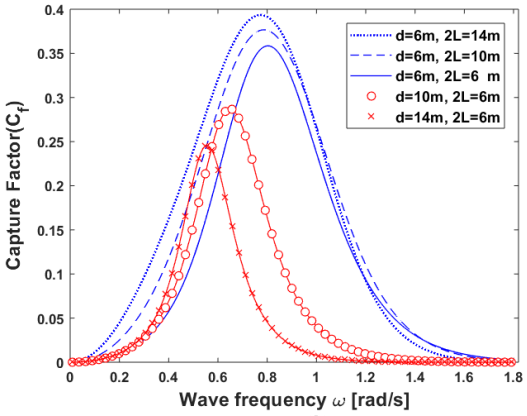

(b)

Figure 9. The variation of a) the output power and b) the capture power versus frequency at different chamber sizes

The capture factor is the efficiency of a power generation device that can be interpreted as the proportion of the output power relative to the input wave power. Since the wave power is dependent on the frequency, the resonant frequency and the trend of the capture factor against the different chamber sizes are not the same as the power one. The resonance frequency of the capture factor compared to those related to power is larger, especially for chambers with a smaller draught. The frequency band around the capture factor's peak and its peak value is reduced by the decrease of the chamber length and, more effectively, is reduced with the increase of the front wall draught.

By comparing the variation of the |Z|, $\overline{P_o}$ and C_F, it can be concluded that the case with a lower amplitude of free surface level has more considerable output power and capture factor. The resonant frequency of the output power is not matched with the one related to water surface displacement, they are different.

Since the power is dependent on the multiplication of $q(t)$ and $p(t)$, the phase difference between these variables is investigated here; a point that has not been comprehensively studied in the previous investigations. If the phase of the Froud-Krylove excitation force, ωt, is considered as the reference, the phases of other variables are expressed as shown in Table 3.

Table 3. The phase difference of the variables of the mathematical model

parameter	Argument or phase
$f(t)_{fr} = F_{fr}e^{i\omega t}$	ωt
$z(t) = \lvert Z\rvert e^{-i\theta}e^{i\omega t}$	$\omega t - \theta$
$\dot{z}(t) = \lvert Z\rvert i\omega e^{-i\theta}e^{i\omega t}$	$\omega t - \theta + \frac{\pi}{2}$
$\ddot{z}(t) = -\lvert Z\rvert\omega^2 e^{-i\theta}e^{i\omega t}$	$\omega t - \theta + \pi$
$\mathrm{q(t)} = Qe^{i\omega t} = S\omega i\lvert Z\rvert . e^{-i\theta}e^{i\omega t}$	$\omega t - \theta + \frac{\pi}{2}$
$\mathrm{p(t)} = Pe^{i\omega t} = \frac{\rho_a S}{\frac{KD}{N} + \frac{V_0}{C^2}\omega i}\omega i\lvert Z\rvert . e^{-i\theta}e^{i\omega t}$	$\omega t - \theta - \theta_1 + \frac{\pi}{2}$ $\theta_1 = \tan^{-1}\left(\frac{V_0 N\omega}{KDC^2}\right)$

For instance, the phase difference between the variables of $z(t), \dot{z}(t), \ddot{z}(t), q(t)$ and $p(t)$ and wave excitation force versus frequency are presented in Figure 10 for two different sizes of chambers, a) $d =$

6 m, $2L = 14$ m, and b) $d = 14$ m, $2L = 6$ m. Based on equation (14), $q(t)$ is dependent on $\dot{z}(t)$ by a positive factor. Therefore, their phase should be the same, a fact that is confirmed in Figure 10 for both cases. Furthermore, the phase difference between $z(t), \dot{z}(t), \ddot{z}(t)$ is respectively 90 degree which is clearly seen. Generally, the phase difference between $q(t)$ and $p(t)$ are approximately the same at low frequencies and increase at larger frequencies. However, it can be concluded that their phase difference is not considerable. It should be noted that although it is expected that at power resonance frequency around 0.5 rad/s, Figure 9-a, the phase difference of $q(t)$ and $p(t)$ would be the smallest value, however, for both chambers this phase difference is not the smallest value as shown in Figure 10. Figure 11 also shows the pressure and flow rate phase versus frequency at different sizes of a rectangular chamber. It is concluded that the change of the chamber draught is more effective than the change of the chamber length on the phase of the pressure and the flow rate.

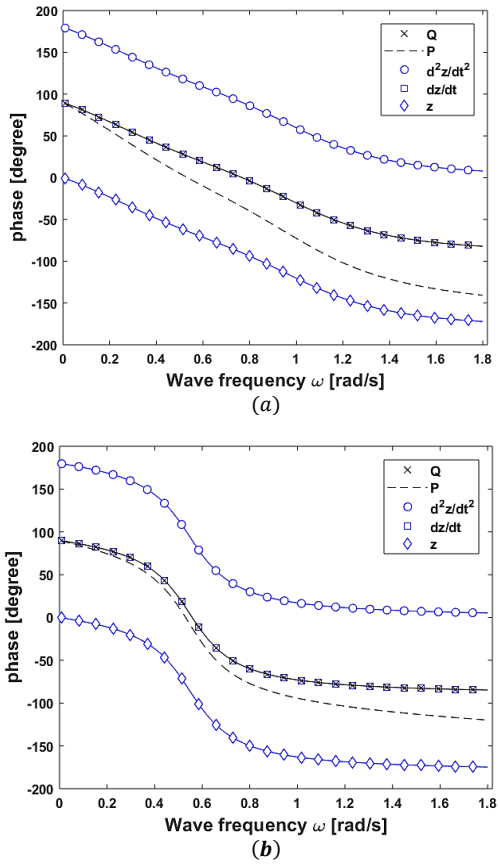

Figure 10. The variation of the phase of variables versus frequency for the case with a) d=6m, 2L=14m, and b) d=14m, 2L=6m

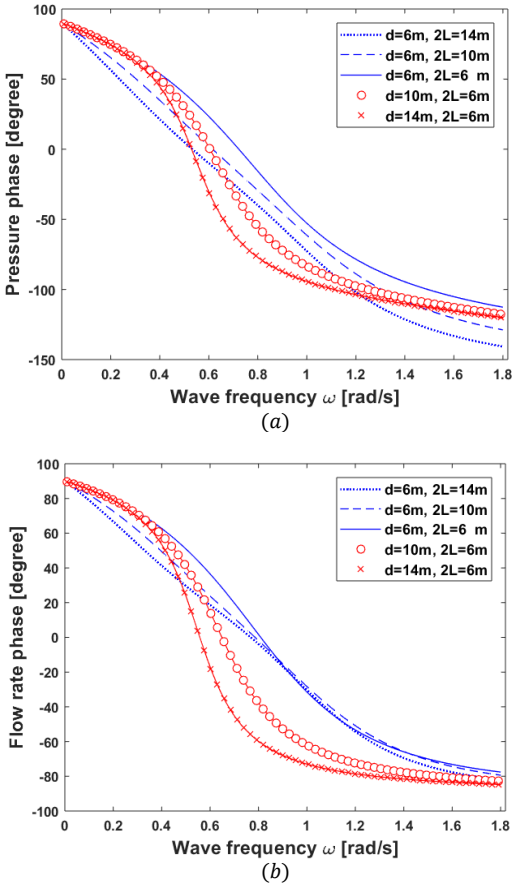

Figure 11. The phase variation of a) the pressure and b) the flow rate versus frequency at different chamber sizes

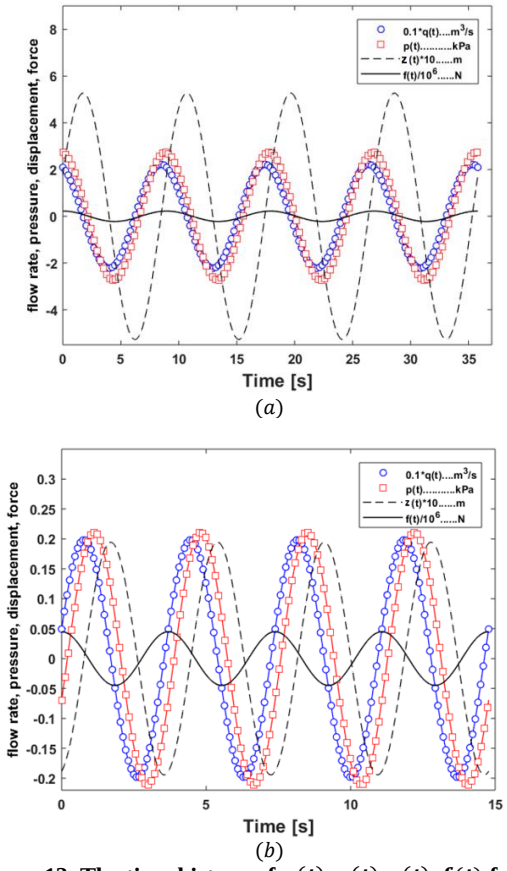

Figure 12. The time history of $q(t), p(t), z(t), f(t)$ for case with $d = 6$m, $2L = 6$m at two frequencies a) $\omega = 0.7$, and b) $\omega = 1.7$

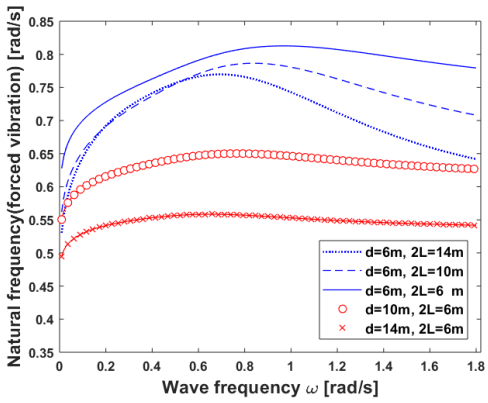

Figure 13. The natural frequency of the forced vibrations

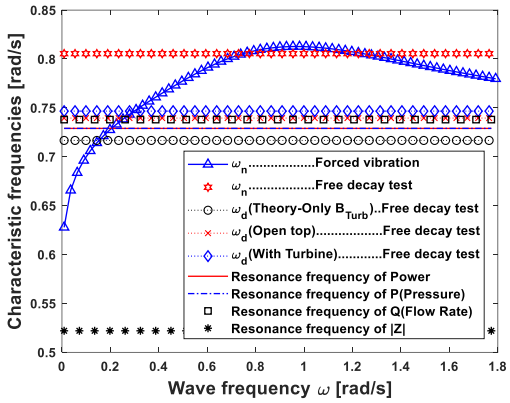

Figure 14. The characteristic frequencies comparison for the case with d=6m, and 2L=6m

To clarify the phase difference between variables, the time history of $q(t), p(t), z(t), f(t)$ are depicted in Figure 12 for the case of $d = 6\,\mathrm{m}, 2L = 6\,\mathrm{m}$ at two values of frequencies. The first one is 0.7 rad/s close to the power resonance frequency, and the second is 1.7 rad/s at a far distance from the power resonance frequency. Figure 12 shows that the phase difference of $q(t)$ and $p(t)$ are obviously higher at high frequency of $\omega = 0.7$ compared to one at frequency close to the power resonance frequency. It is observed that the phase difference between $q(t)$ and $p(t)$ is not exactly zero around the power resonant frequency.

Now the variation of the forced natural frequency is investigated as presented in Figure 13. Since the stiffness is constant, the forced natural frequency is inversely proportional to equivalent mass. The change of the chamber length does not change the natural frequency considerably while increasing the chamber draught decreases the forced natural frequency. It should be noted that at high excitation frequencies, the chamber length effect is considerable. The case with a longer length causes higher natural frequencies in a forced vibration condition.

The comparison of all the introduced characteristic frequencies of the free decay test and force vibration is presented in Figure 14-Figure 16 for different sizes of the rectangular chamber. The results show that when the chamber has different sizes, the first indicator of resonant frequencies of the power is the pressure resonance frequency because they are exactly in agreement. For the second indicator, the resonance frequency of the flow rate can be suggested. However, the mentioned indicators are difficult to calculate. Regarding the other simple indicator, surprisingly, the damped natural frequency of the open-top case is closer to the power resonant frequency than other defined damped frequencies. The computed damped frequency for "with turbine" and "Theory-only B_{Turb}" cases have similar strength for estimating the power resonant frequency.

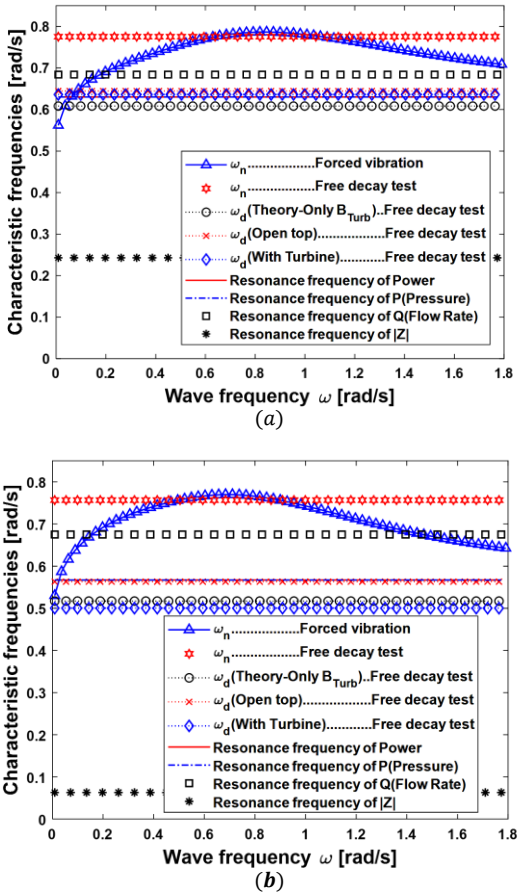

Figure 15. The Comparison of the characteristic frequencies for cases with a) d=6m, 2L=10m, and b) d=6m, 2L=14m

It is clear that the defined natural frequency, ω_n, of the free decay test and the forced vibration is not suggested as an accurate indicator. Furthermore, the resonant frequency of the water level displacement in the forced vibration is very far from the defined natural frequency and the damped frequencies of the free decay test. Therefore, approximately all of the damped natural frequencies, especially the open-top, are suggested for determining the power resonant frequencies.

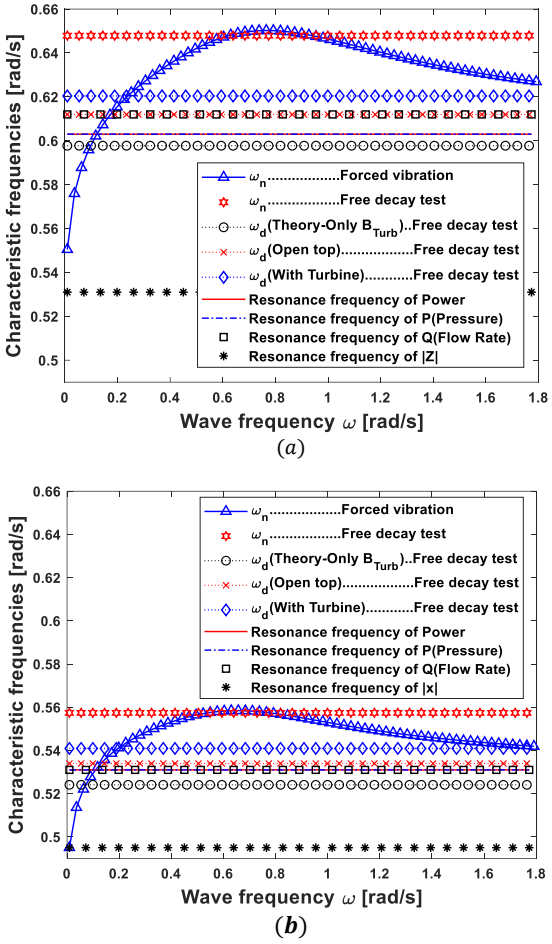

Figure 16. The Comparison of the characteristic frequencies for cases with a) d=10m, 2L=6m, and b) d=14m, 2L=6m

7. Conclusion

In the present study, a frequency domain analysis based on the RLC circuit model is utilized for solving the linearized governing equation of an OWC wave energy converter based on the simplified rigid piston model. The system is modeled as an SDOF-MSD. The results of this mathematical model are summarized as:

1- The observed trends of the pressure, the flow rate, and the displacement of the free surface versus frequency are properly in agreement with the predicted actual condition.
2- The case with a lower amplitude of the free surface level has higher output power and capture factor, which is observed by comparing the resulting curves.
3- The phase difference between the pressure and the flow rate is not the smallest value at the power resonance frequency.
4- The resonant frequency of the power and the pressure are approximately the same. They can be estimated with the frequency value of the free decay test in two conditions; the applied turbine and in an open-top condition without a turbine. For the considered dimensions, the resonant frequency is around 5-7 rad/s, equivalent to periods of 8.5-12.5 s. This wave period is approximately around wave dominant periods, confirming the design works well.

8. References

1- EVANS, D.,(1978), *The oscillating water column wave-energy device*, IMA Journal of Applied Mathematics, 22(4), p. 423-433.
2- BRENDMO, A., FALNES, J. and LILLEBEKKEN, P.,(1996), *Lineår modelling of oscillating water columns including viscous loss*, Applied Ocean Research, 18(2-3), p. 65-75.
3- LOPES, M., *et al.*,(2009), *Experimental and numerical investigation of non-predictive phase-control strategies for a point-absorbing wave energy converter*, Ocean Engineering, 36(5), p. 386-402.
4- FALCÃO, A. F., HENRIQUES, J. C. and CÂNDIDO, J. J.,(2012), *Dynamics and optimization of the OWC spar buoy wave energy converter*, Renewable Energy, 48, p. 369-381.
5- KETABDARI, M. and AKHTARI, A.,(2012), *Numerical modeling of oscillating water column wave energy convertor*, International Journal of Advanced renewable energy research, 1(4).
6- SUZUKI, M., WASHIO, Y. and KUBOKI, T.,(2005), in *The Fifteenth International Offshore and Polar Engineering Conference*. OnePetro.
7- MARTINS-RIVAS, H. and MEI, C. C.,(2009), *Wave power extraction from an oscillating water column at the tip of a breakwater*, Journal of Fluid Mechanics, 626, p. 395-414.
8- EVANS, D. V. and PORTER, R.,(1997), *Efficient calculation of hydrodynamic properties of OWC-type devices*.
9- ŞENTÜRK, U. and ÖZDAMAR, A.,(2012), *Wave energy extraction by an oscillating water column with a gap on the fully submerged front wall*, Applied Ocean Research, 37, p. 174-182.
10- HAI, L., GÖTEMAN, M. and LEIJON, M.,(2016), *A methodology of modelling a wave power system via an equivalent RLC circuit*, IEEE Transactions on Sustainable Energy, 7(4), p. 1362-1370.
11- HAI, L., SVENSSON, O., ISBERG, J. and LEIJON, M.,(2015), *Modelling a point absorbing wave energy converter by the equivalent electric circuit theory: A feasibility study*, Journal of Applied Physics, 117(16), p. 164901.
12- ZHAO, H.-T., SUN, Z.-L., HAO, C.-L. and SHEN, J.-F.,(2013), *Numerical modeling on hydrodynamic performance of a bottom-hinged flap wave energy converter*, China Ocean Engineering, 27(1), p. 73-86.
13- FARSANGI, M. A. A. and ZOHOOR, H.,(2019), *Acoustic energy harvesting via magnetic shape memory alloys*, Journal of Physics D: Applied Physics, 52(13), p. 135501.
14- SIMONETTI, I., CAPPIETTI, L., EL SAFTI, H. and OUMERACI, H.,(2015), in *International Conference on Offshore Mechanics and Arctic*

Engineering. American Society of Mechanical Engineers, vol. 56574, p. V009T009A031.
15- VYZIKAS, T., DESHOULIÈRES, S., GIROUX, O., BARTON, M. and GREAVES, D.,(2017), *Numerical study of fixed Oscillating Water Column with RANS-type two-phase CFD model,* Renewable Energy, 102, p. 294-305.
16- ELHANAFI, A., FLEMING, A., MACFARLANE, G. and LEONG, Z.,(2017), *Underwater geometrical impact on the hydrodynamic performance of an offshore oscillating water column–wave energy converter,* Renewable Energy, 105, p. 209-231.
17- ÇELIK, A. and ALTUNKAYNAK, A.,(2020), *Determination of damping coefficient experimentally and mathematical vibration modelling of OWC surface fluctuations,* Renewable Energy, 147, p. 1909-1920.
18- ÇELIK, A. and ALTUNKAYNAK, A.,(2020), *Determination of hydrodynamic parameters of a fixed OWC by performing experimental and numerical free decay tests,* Ocean Engineering, 204, p. 106827.
19- ÇELIK, A. and ALTUNKAYNAK, A.,(2020), *Estimation of water column surface displacement of a fixed oscillating water column by simple mechanical model with determination of hydrodynamic parameters via physical experimental model,* Journal of Waterway, Port, Coastal, and Ocean Engineering, 146(5), p. 04020030.
20- PORTILLO, J., *et al.*,(2020), *Wave energy converter physical model design and testing: The case of floating oscillating-water-columns,* Applied Energy, 278, p. 115638.
21- FALTINSEN, O.,(1993), *Sea loads on ships and offshore structures*, Cambridge university press, vol. 1.
22- FALCÃO, A. D. O. and JUSTINO, P.,(1999), *OWC wave energy devices with air flow control,* Ocean Engineering, 26(12), p. 1275-1295.
23- GOMES, R., HENRIQUES, J., GATO, L. and FALCÃO, A. D. O.,(2012), *Hydrodynamic optimization of an axisymmetric floating oscillating water column for wave energy conversion,* Renewable Energy, 44, p. 328-339.
24- ABAZARI, A.,(2022), *Dynamic Response of a Combined Spar-Type FOWT and OWC-WEC by a Simplified Approach,* Renewable Energy Research and Applications.